Purcell's swimmer in a shear-thinning fluid

Ke Qin and On Shun Pak
Department of Mechanical Engineering, Santa Clara University, Santa Clara, California 95053, USA

(Received 8 July 2022; accepted 31 January 2023; published 3 March 2023)

Locomotion of biological and artificial microswimmers has received considerable attention due to its fundamental biological relevance and promising biomedical applications such as drug delivery and microsurgery. Purcell's well-known discussion on "Life at Low Reynolds Number" [Am. J. Phys. **45**, 3 (1977)] elucidated the stringent fluid dynamical constraints on swimming at the microscopic scale. He also presented the "simplest animal," now known as Purcell's swimmer, that can swim in the absence of inertia, which has now become a useful model for exploring different fundamental aspects of microscopic locomotion. While extensive studies have improved our understanding of locomotion in Newtonian fluids, microswimmers often encounter biological fluids that display complex (non-Newtonian) rheological behaviors, and much less is known about swimming in complex fluids. In this work, we utilize Purcell's swimmer as a model swimmer to probe the impacts of shear-thinning rheology, a ubiquitous non-Newtonian behavior of biological fluids such as blood and mucus, on swimming at low Reynolds numbers. We show how the propulsion characteristics of Purcell's swimmer in a shear-thinning fluid differ from those in a Newtonian fluid in terms of both the magnitude and direction of propulsion, depending on the details of the swimming strokes. The simplicity of Purcell's swimmer allows us to rationalize the results by examining how the shear-thinning effect manifests in different swimming strokes in a cycle. We also demonstrate how unequal arm rotational rates can couple with the shear-thinning effect to induce a net vertical displacement of the swimmer, which is not possible in a Newtonian fluid. These results suggest modulating the arm rotational rates as a way to enable different two-dimensional motions of Purcell's swimmer in a shear-thinning fluid.

DOI: 10.1103/PhysRevFluids.8.033301

I. INTRODUCTION

Microscopic locomotion has attracted considerable recent attention for both the important roles of swimming cells in diverse biological processes [1–4] and the potential biomedical applications of artificial microswimmers [5–8]. Purcell's well-known discussion on "Life at Low Reynolds Number" [9] elucidated the fundamental fluid dynamical constraints on swimming at low Reynolds numbers. For instance, now known as the scallop theorem, no reciprocal motion (i.e., sequence of motions with time-reversal symmetry), such as a single-hinged scallop opening and closing its shell, can lead to net displacement as a consequence of the linearity and time independence of the Stokes equations. Common macroscopic locomotion strategies such as a rigid flapping motion therefore become ineffective at the microscopic scale. Microorganisms have evolved different strategies to swim in the microscopic world. For instance, flagellated bacteria swim via the use of rotary motors powered by ion fluxes to rotate helical filaments; some sperm cells utilize the action of molecular motors within flagella to generate bending waves traveling along their flagellum for swimming. Extensive studies over the past several decades have led to an improved understanding of the hydrodynamics underlying their motility [10–12]. However, without complex molecular machinery empowering cell motility, the design of simple mechanisms that can overcome the

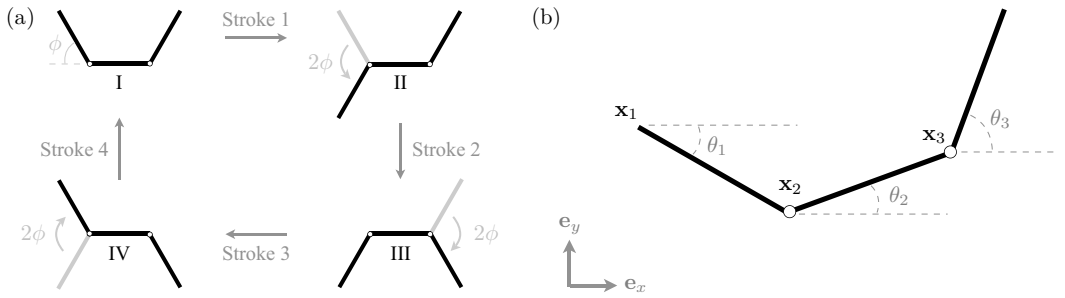

FIG. 1. (a) The four arm strokes of Purcell's swimmer. (b) Notations for describing the motion of Purcell's swimmer in the *x*-*y* plane.

stringent constraints on low-Reynolds-number swimming represents a fundamental challenge in the development of artificial microswimmers [13].

Purcell presented an elegant example of the "simplest animal," now known as Purcell's swimmer, that can generate net translation with kinematically irreversible cyclic motions [9]. The swimmer consists of three rigid links connected by two hinges. The middle link is connected to two other links (arms) which take turns rotating relative to the middle link to undergo the four arm strokes illustrated in Fig. 1(a). Symmetry arguments concluded that such a linkage would move in a straight line over one cycle [9]. Although the direction of net displacement was left as an exercise for the readers, the answer was not obvious [14] until a detailed analysis of the swimmer by Becker *et al.* [15]. Purcell's swimmer has now been widely adopted as a useful model for exploring various fundamental aspects of swimming at low Reynolds numbers [15–17], optimal locomotion [18–20], and the effect of swimmer elasticity [21,22]. The model was also studied as the simplest inertialess swimmer in granular media [23]. Furthermore, a possible connection between the locomotion of the helical bacteria *Spiroplasmas* and Purcell's swimmer was suggested [15,24].

Here, we employ Purcell's swimmer to probe the impact of shear-thinning rheology on swimming at low Reynolds numbers. Many microorganisms often encounter biological fluids that display non-Newtonian rheological behaviors, including viscoelasticity and shear-thinning viscosity. To better understand their locomotion and to guide the design of artificial microswimmers for biomedical applications, it is important to examine how different complex rheological properties of biological fluids influence locomotion [8]. While considerable efforts have focused on swimming in viscoelastic fluids [25,26], the effect of shear-thinning rheology has been studied only more recently. A shear-thinning fluid such as blood and mucus [27,28] loses its viscosity with increased shear rates. The shear-thinning effect can either hinder or enhance propulsion, depending on the specific types of swimmers (e.g., undulatory swimmers [29–37], helical swimmers [38–40], and squirmers [30,41–44], among others [29,30,45]) and the details of their swimming gaits. Various theories have been proposed to explain the physical mechanisms underlying the speed hindrance and enhancement. In particular, the shear-thinning effect can hinder the swimming of undulatory filaments by reducing the thrust more than drag [37], whereas the speed enhancements in undulatory sheets [34] and helical swimmers [38,40] have been attributed to a soft confinement effect due to the presence of a low-viscosity region surrounding the swimmer. The non-Newtonian effect has also been used to demonstrate the breakdown of the scallop theorem by enabling the swimming of a single-hinged scallop in a shear-thinning fluid [46,47]. Findings from these recent studies suggest that when and why a swimmer goes faster or slower in a shear-thinning fluid highly depend on the specific types of swimmers. In this work, we examine the effect of shear-thinning rheology on the motion of Purcell's swimmer. The simplicity of Purcell's swimmer allows us to rationalize the results by examining how the shear-thinning effect manifests in different swimming strokes, leading to the overall changes in the swimmer displacement. Our results show that shear-thinning rheology impacts not only the magnitude but also the direction of propulsion of Purcell's swimmer. In addition, while Purcell's

swimmer can generate only net movements in a single direction in a Newtonian fluid [9,15], here, we explore the possibility of exploiting the shear-thinning effect to enable two-dimensional motion. Taken together, the analysis of this canonical swimmer here contributes another specific example to illustrate different consequences that shear-thinning rheology can have on microswimmers.

This paper is organized as follows. In Sec. II, we describe in more detail Purcell's three-link swimmer model (Sec. II A) and formulate the equations governing its motion in a shear-thinning fluid (Sec. II B). In Sec. III, we first revisit the results in the Newtonian limit (Sec. III A), which lay the foundation for understanding the effect of shear-thinning in Sec. III B and the new dynamics emerging from symmetry breaking in Sec. III C. Finally, we conclude this work with remarks on its limitations and directions of future work in Sec. IV.

II. PROBLEM FORMULATION

A. Swimmer model

We consider a Purcell's swimmer of a total length L, which consists of three slender, rigid links (each with length $\ell = L/3$ and radius a) connected by two hinges with negligible hydrodynamic effects. In its initial configuration, the middle link is connected to the left and right links (arms) symmetrically at an angle ϕ [configuration I in Fig. 1(a)]. The swimmer performs four arm strokes to complete a swimming cycle. During these strokes, the swimmer alternately rotates its left or right link (arm) relative to the middle link by a fixed angle ($\pm 2\phi$) in the clockwise (+) or counterclockwise (−) direction [Fig. 1(a)] at a constant rotational rate ω: In stroke 1, the swimmer rotates its left arm in the counterclockwise direction. In stroke 2, the swimmer rotates its right arm in the clockwise direction. In stroke 3, the swimmer rotates its left arm in the clockwise direction. Finally, in stroke 4, the swimmer rotates its right arm in the counterclockwise direction to return to its original configuration, completing the swimming cycle.

The motion of the swimmer occurs in the x-y plane spanned by the basis vectors $\mathbf{e}_x$ and $\mathbf{e}_y$. The ith link ($i = 1, 2, 3$) is specified by the position vector of its left end $\mathbf{x}_i = x_i\mathbf{e}_x + y_i\mathbf{e}_y$ and the angle θ_i made between its tangent vector $\mathbf{t}_i = \cos\theta_i\mathbf{e}_x + \sin\theta_i\mathbf{e}_y$ and $\mathbf{e}_x$ [Fig. 1(b)]. A point along the ith link is therefore given by $\mathbf{X}_i(s, t) = \mathbf{x}_i + s\mathbf{t}_i$, where $s \in [0, \ell]$ is the arclength parameter along the link.

B. Governing equations

The hydrodynamic force on a slender body at low Reynolds numbers in a Newtonian fluid can be described by the leading-order slender-body approximation known as the resistive force theory (RFT) [48,49], which assumes nonlocal hydrodynamic interactions between different parts of the slender body are negligible. As a local drag model, RFT linearly relates, in a tensorial fashion, the hydrodynamic force density along the slender body to its local velocity. More recently, Riley and Lauga [37] proposed a modified RFT for studying the locomotion of slender bodies in a shear-thinning fluid. Here, we apply the modified RFT to describe the hydrodynamics of the slender, rigid links in Purcell's swimmer. The hydrodynamic force density on the ith link is given by

$$\mathbf{f}_i = -R_C(t, \mathbf{X}_i)[\xi_\perp(\mathbf{I} - \mathbf{t}_i\mathbf{t}_i) + \xi_\parallel\mathbf{t}_i\mathbf{t}_i] \cdot \mathbf{u}_i, \tag{1}$$

where $\mathbf{u}_i = \partial\mathbf{X}_i/\partial t$ is the local velocity along the link, $\xi_\parallel = 2\pi\eta_0/[\ln(L/a) - 1/2]$ and $\xi_\perp = 4\pi\eta_0/[\ln(L/a) + 1/2]$ are the classical RFT coefficients in a Newtonian fluid with dynamic viscosity η_0 [48,49], and $\mathbf{I}$ is the identity tensor. Here, R_C is a correction factor accounting for the local shear-thinning effect based on the Carreau constitutive model [37,50]

$$R_C(t, \mathbf{X}_i) = [1 + (\lambda_C\dot{\gamma}_{\text{avg}})^2]^{(n-1)/2}, \tag{2}$$

where $1/\lambda_C$ represents a critical shear rate beyond which the shear-thinning effects become significant and n is the shear-thinning index. For biological fluids [32,51–53], the value of λ_C can span a wide range, on the order of 0.1–100 s, with n in the range of 0.1–0.8. For xanthan gum solutions

with different concentrations [33,54], λ_C can vary between 0.1 and 10 s, with n in the range of 0.3–0.9. Here, $\dot{\gamma}_{\text{avg}}$ is the local average shear rate around a slender body, given by

$$\dot{\gamma}_{\text{avg}} = \frac{\sqrt{\xi_\perp^2 u_\perp^2 + 2\xi_\parallel^2 u_\parallel^2}}{2\sqrt{2}a\pi\eta_0}. \tag{3}$$

The local shear rate varies along the body depending on the tangential ($u_\parallel$) and normal ($u_\perp$) velocity components. The correction factor R_C therefore varies both spatially and temporally along the swimmer.

The total hydrodynamic force on the ith link of Purcell's swimmer is therefore given by

$$\mathbf{F}_i = \int_0^\ell \mathbf{f}_i(\mathbf{X}_i)\, ds, \tag{4}$$

and the total hydrodynamic torque on the ith link about $\mathbf{x}_j$ is given by

$$\mathbf{T}_{i,j} = \int_0^\ell (\mathbf{X}_i - \mathbf{x}_j) \times \mathbf{f}_i(\mathbf{X}_i)\, ds. \tag{5}$$

Finally, the set of equations describing the dynamics of Purcell's swimmer is closed with the overall force-free and torque-free conditions,

$$\sum_{i=1}^{3} \mathbf{F}_i = \mathbf{0}, \quad \sum_{i=1}^{3} \mathbf{T}_{i,1} = \mathbf{0}, \tag{6}$$

for a free swimmer at low Reynolds numbers.

In this work we nondimensionalize lengths by L, time by $1/\omega$, and forces by $L^2\xi_\perp\omega$. In dimensionless form, the correction factor R_C is given by

$$R_C = \left(1 + \text{Cu}^2\, \tilde{\dot{\gamma}}_{\text{avg}}^2\right)^{(n-1)/2}, \tag{7}$$

where $\tilde{\dot{\gamma}}_{\text{avg}}$ is the dimensionless local average shear rate and $\text{Cu} = \omega\lambda_C$ is the Carreau number comparing the characteristic rotational rate ω with the critical shear rate $1/\lambda_C$. For the slender-body approximation to be valid, we set a small slenderness ratio of $a/L = 1/1000$ in this work. Hereafter, we use the same notations for the corresponding dimensionless variables and refer to only dimensionless variables unless otherwise stated.

For numerical implementation, we use the numerical routine FSOLVE in the SCIPY library, a root-finding algorithm based on the Powell hybrid method [55], to solve the equations of force and torque balances [Eq. (6)] for the translational velocity $\dot{\mathbf{x}}_1$ and angular velocity $\dot{\theta}_1$, with a relative tolerance of 1×10^{-10}. We then obtain the updated position $\mathbf{x}_1$ and orientation θ_1 by solving the first-order system with $\dot{\mathbf{x}}_1$ and $\dot{\theta}_1$ using LSODA [56,57] from the ODEPACK library through the ODEINT routine with a relative tolerance of 1×10^{-9}. The remaining position vectors $\mathbf{x}_i$ and angles θ_i ($i = 2, 3$) are then determined by the prescribed kinematics of the linkage.

We remark on the regime of validity of the modified RFT in a shear-thinning fluid: In order to be self-consistent with the local nature of the RFT, the shear-thinning effect on the viscosity around each section of the slender body should also be local (i.e., caused by the local movement of the body) [32]. This requires the shear rate at the relevant length over which the slender body can be approximated as straight (taken as ω) to be smaller than the critical shear rate ($1/\lambda_C$), i.e., $\text{Cu} = \omega\lambda_C < 1$, limiting the validity of the current model to the low-Carreau-number regime. We therefore confine our investigation to only small values of the Carreau number ($\text{Cu} \leqslant 0.1$) in this work.

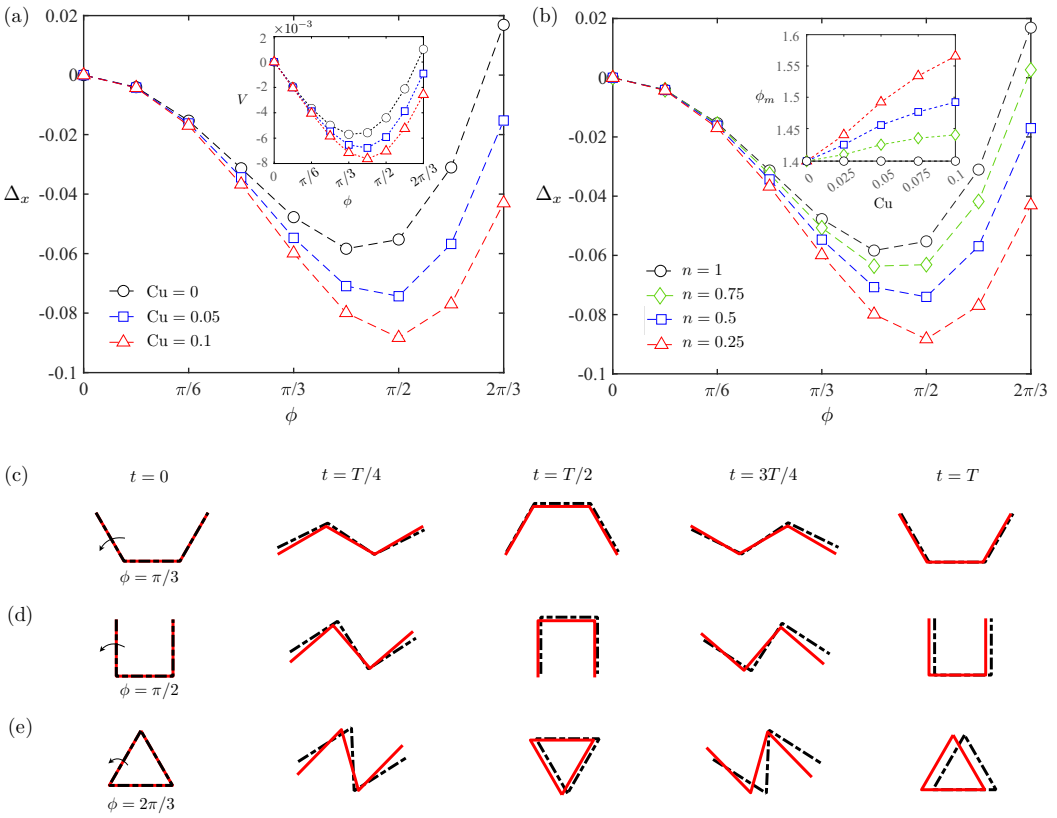

FIG. 2. Propulsion performance of Purcell's swimmer characterized by (a) the net horizontal swimmer displacement Δ_x and (inset) the average swimming velocity V as a function of the stroke angle ϕ in Newtonian (Cu = 0) and shear-thinning (Cu = 0.05, Cu = 0.1) fluids with $n = 0.25$. (b) The variation of Δ_x as a function of ϕ at different values of n with Cu = 0.1; inset: the stroke angle ϕ_m that maximizes the magnitude of Δ_x at different values of Cu and n. (c)–(e) The shape and orientation of the linkage when the swimmer completes individual strokes ($t = 0,\ T/4,\ T/2,\ 3T/4,\ T$) are compared for the Newtonian (black dash-dotted lines, Cu = 0) and shear-thinning (red solid lines, Cu = 0.1) cases for different stroke angles: (c) $\phi = \pi/3$, (d) $\phi = \pi/2$, and (e) $\phi = 2\pi/3$.

III. RESULTS AND DISCUSSION

We apply the framework described in Sec. II B to examine the propulsion of Purcell's swimmer in a shear-thinning fluid. The displacement of the center of the middle link, denoted as $[D_x(t), D_y(t)] = \mathbf{X}_2(s = \ell/2,\ t)$, is used to track the swimmer displacement. After the prescribed strokes in a swimming cycle of period T are performed, the net horizontal and vertical displacements of the swimmer are, respectively, given by $\Delta_x = D_x(t+T) - D_x(t)$ and $\Delta_y = D_y(t+T) - D_y(t)$. In the following, we first revisit results for the dynamics of Purcell's swimmer in a Newtonian fluid (Sec. III A), which lay the foundation for understanding the effect of shear-thinning rheology in Secs. III B and III C.

A. Newtonian results

We first reproduce the results in the Newtonian limit [15] by considering a vanishing Carreau number, Cu = 0. Because of symmetry considerations (see further details in [9,15] and a summary of the discussion below), the swimmer can displace itself only horizontally ($\Delta_y = 0$). In Fig. 2(a),

the net horizontal displacement of the swimmer after a cycle Δ_x is displayed as a function of the stroke angle ϕ in a Newtonian fluid (black circles). The propulsion direction of Purcell's swimmer, left as an exercise for readers by Purcell [9] and analyzed in detail by Becker *et al.* [15], can, indeed, be either to the left ($\Delta_x < 0$) or to the right ($\Delta_x > 0$), depending on ϕ. The magnitude of the displacement $|\Delta_x|$ varies nonmonotonically with the stroke angle ϕ: $|\Delta_x|$ first increases with ϕ, reaching a maximum between $\pi/3$ and $\pi/2$, and then decreases to zero, before a switch in the propulsion direction to the positive x direction (to the right) with a sufficiently large stroke angle (e.g., $\phi = 2\pi/3$). As a remark, given the same arm rotational rates, the time period T required for a Purcell's swimmer to complete a swimming cycle varies with the stroke angle. One may therefore also measure the propulsion performance by defining an average swimming velocity, $V = \Delta_x/T$, over one period of the swimming cycle, as shown in the inset in Fig. 2(a), which shows features qualitatively similar to the net swimmer displacement. We also remark that the parametric study here is performed only up to $\phi = 2\pi/3$, beyond which the swimmer's two arms would cross each other, as illustrated in Fig. 2(e). Moreover, since a local drag model is employed here, the results are expected to be less accurate for large values of ϕ, where the links become close in proximity and nonlocal hydrodynamic interactions would become important. In Figs. 2(c)–2(e), we display the motion of Purcell's swimmer with different stroke angles at different time instants in a swimming cycle. The propulsion characteristics of Purcell's swimmer in a Newtonian fluid were qualitatively explained in detail based on the drag anisotropy of the links and the orientation of the linkages by Becker *et al.* [15]. Below, we revisit some of these ideas, which are essential for understanding the impact of shear-thinning rheology on the propulsion of Purcell's swimmer in the following sections.

In explaining the propulsion of Purcell's swimmer, one can focus on the first stroke of the swimming cycle [stroke 1 in Fig. 1(a); $t = 0$ to $t = T/4$ in Figs. 3(a) and 3(b)] because the remaining strokes (strokes 2–4) follow from the first stroke via symmetry considerations [15]; for example, stroke 2 is related to stroke 1 through a combination of time-reversal and rotational symmetries. These symmetry considerations imply that the horizontal displacements of the center of the middle link $\Delta_{x,n}$ resulting from the nth stroke are identical: $\Delta_{x,1} = \Delta_{x,2} = \Delta_{x,3} = \Delta_{x,4}$; the corresponding vertical displacements $\Delta_{y,n}$ are given by $\Delta_{y,1} = \Delta_{y,2} = -\Delta_{y,3} = -\Delta_{y,4}$, leading to zero net vertical displacement of the swimmer after a swimming cycle. The detailed time evolution of the displacement of the middle link's center, D_x and D_y, are shown in Figs. 3(a) and 3(b), verifying these symmetry properties.

It is therefore sufficient to consider the first stroke in the following discussion: In stroke 1 [Figs. 3(c) and 3(d)], the left arm rotates counterclockwise, and the remaining structure (middle link and right arm) rotates in the opposite direction to maintain an overall torque-free condition. In the initial phase of the stroke, i.e., before the left arm reaches the horizontal level [Fig. 3(d), (i)–(iii)], the counterclockwise rotation of the left arm acts to displace the swimmer to the right; meanwhile, the clockwise rotation of the right arm acts to displace the swimmer in the opposite direction, which initially lessens the swimmer's overall displacement to the right [Fig. 3(d), (i) and (ii)] and eventually causes the swimmer to move to the left [Fig. 3(d), (ii) and (iii)]. In the remaining phase of the stroke, i.e., after the left arm moves past the horizontal level [Fig. 3(d), (iii) and (iv)], both the counterclockwise rotation of the left arm and the clockwise rotation of the right arm act in tandem to displace the swimmer to the left. Overall, we note that while the displacement caused by the counterclockwise rotation of the left arm switches direction during the stroke, the clockwise rotation of the right arm always acts to displace the swimmer to the left. As shown in Fig. 3(c), the overall displacement of the swimmer is to the left after the first stroke. Since the remaining strokes follow from the first strokes by symmetries ($\Delta_{x,1} = \Delta_{x,2} = \Delta_{x,3} = \Delta_{x,4}$), the swimmer moves to the left at the end of the swimming cycle [Fig. 3(a)].

The above discussion focuses only on the motion of the left and right arms. As discussed by Becker *et al.* [15], the propulsion of Purcell's swimmer is affected not only by the motion of the two arms but also that of the middle link. When the stroke angle is small, the latter effect is secondary due to the small inclinations of the middle link relative to the horizontal level and its relatively low velocities. For larger stroke angles, however, the inclination of the middle link becomes significant

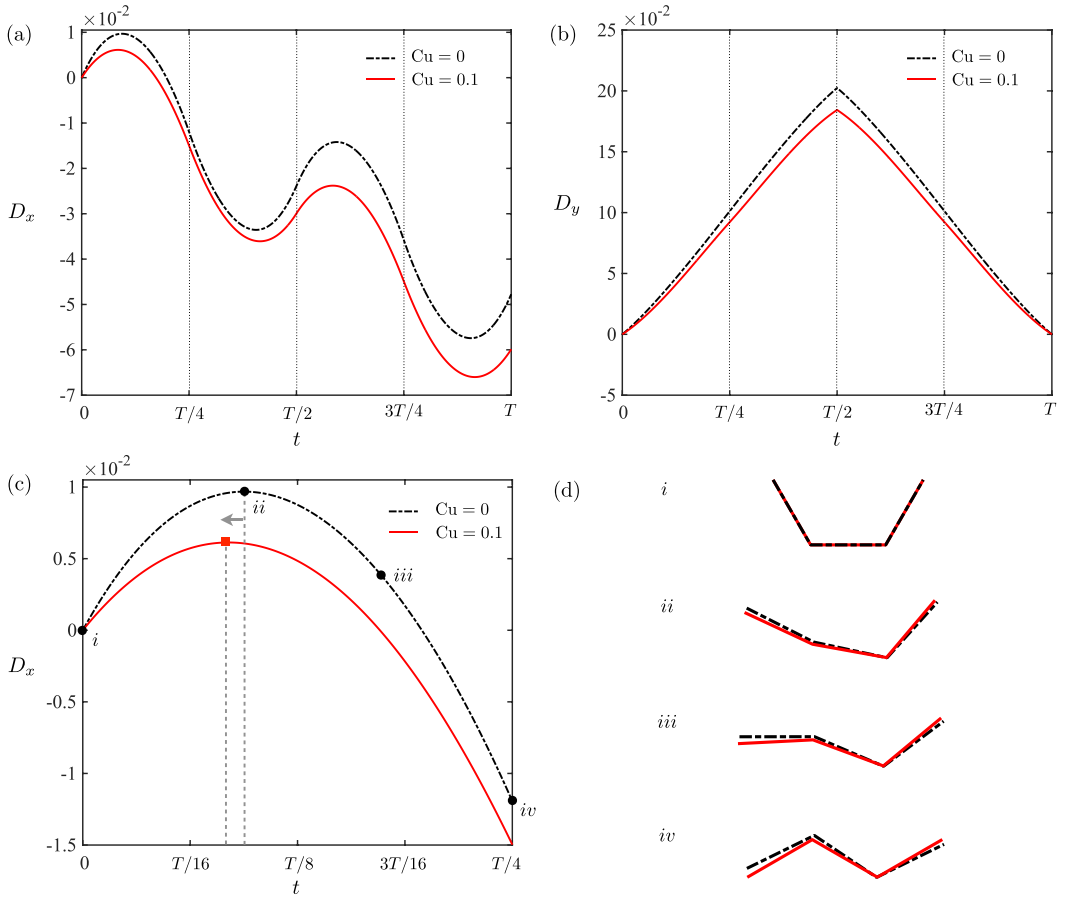

FIG. 3. The displacement of the middle link's center in the (a) horizontal (D_x) and (b) vertical (D_y) directions as a function of time t in a swimming cycle. In (c), the dashed lines indicate the time instants when the swimmer switches its swimming direction from rightward to leftward in the first stroke ($t = 0$ to $t = T/4$). (d) displays the shape and orientation of the linkage at different representative time instants from the start (i) to the end (iv) of the first stroke as indicated in (c). Here (ii) is the time instant when the swimmer in a Newtonian fluid starts to switch its swimming direction from rightward to leftward; (iii) is the time instant when the left arm of the swimmer in a Newtonian fluid becomes horizontal and starts to contribute to leftward displacement. The swimmer at the same time instants in a shear-thinning fluid is shown for comparison. In all panels, $\phi = \pi/3$, and the black dash-dotted lines and red solid lines represent Newtonian (Cu = 0) and shear-thinning (Cu = 0.1) results, respectively. Here, $n = 0.25$.

enough to affect the swimmer's displacement, leading to the nonmonotonic variation of swimmer displacement shown in Fig. 2(a) and even a change in swimming direction when $\phi = 2\pi/3$.

B. Effect of shear-thinning rheology

We now examine the impact of shear-thinning rheology on the propulsion of Purcell's swimmer. As shown in Fig. 2(a), the shear-thinning effect (Cu = 0.05, Cu = 0.1) acts to favor the propulsion of Purcell's swimmer in the negative x direction (to the left). That is, for stroke angles where Purcell's swimmer moves to the left in a Newtonian fluid, the swimmer moves farther to the left in a shear-thinning fluid; when $\phi = 2\pi/3$, where Purcell's swimmer moves to the right in a

Newtonian fluid, shear-thinning rheology can lead to a change in the swimming direction, causing the swimmer to move to the left instead. Similar qualitative features are observed in Fig. 2(b) when the fluid becomes more shear thinning as the shear-thinning index n decreases from unity. In the Newtonian case (Cu $= 0$ or $n = 1$), a stroke angle ϕ_m exists that maximizes the magnitude of the swimmer displacement Δ_x. We note that shear-thinning rheology modifies ϕ_m for different values of Cu > 0 and $n < 1$. Specifically, in the inset in Fig. 2(b), we show that ϕ_m increases when the fluid becomes more shear thinning (i.e., when Cu increases or when n decreases). In Figs. 2(c)–2(d), we contrast the motion of Purcell's swimmer in a Newtonian fluid (black dot-dashed lines) with that in a shear-thinning fluid (Cu $= 0.1$, red solid lines) at the end of individual strokes in a swimming cycle. As will be explained below, shear-thinning rheology alters the orientation of the linkages in manners that favor swimmer displacement to the left. The detailed time evolutions of the horizontal and vertical displacements, D_x and D_y, of the swimmer in a shear-thinning fluid are shown (red solid lines) in Figs. 3(a) and 3(b). From these results, we verify numerically that, in spite of the shear-thinning effect, Purcell's swimmer still retains the properties $\Delta_{x,1} = \Delta_{x,2} = \Delta_{x,3} = \Delta_{x,4}$ and $\Delta_{y,1} = \Delta_{y,2} = -\Delta_{y,3} = -\Delta_{y,4}$, which means that the net swimmer displacement remains in the horizontal direction and it is still sufficient to focus on the first stroke of the swimming cycle to understand the swimmer dynamics in a shear-thinning fluid.

The enhanced displacement of Purcell's swimmer to the left may be rationalized by a detailed examination of the changes in the displacement and orientation of the linkage due to shear-thinning rheology in the first stroke of the swimming cycle [Figs. 3(c) and 3(d)]. Due to the smaller rotational resistance of the left arm relative to the remaining structure (middle link and the right arm), a higher rotational rate and hence higher shear rates in the fluid around the left arm than in that around the right arm are expected. A stronger shear-thinning effect thus occurs around the left arm than around the right arm, causing the left arm to rotate more in the counterclockwise direction and the right arm to rotate less in the clockwise direction [red solid lines in Fig. 3(d)], relative to the Newtonian case (black dash-dotted lines). Both of these changes favor the swimmer displacement to the left: The left arm spends more time in the phase moving past the horizontal level, and the increased vertical alignment of the left arm due to its further counterclockwise rotation [Fig. 3(d), (iv)] promotes leftward displacement. Similarly, the reduced clockwise rotation of the right arm allows it to remain more vertically aligned and thereby to contribute more to the leftward displacement of the swimmer throughout the stroke. These effects result in an earlier switch of the direction of the swimmer displacement, as indicated in Fig. 3(c), favoring the displacement of the swimmer to the left. Since the remaining strokes follow from the first stroke, the swimmer overall has an increased net displacement in the negative x direction (to the left) in a shear-thinning fluid, as shown in Fig. 3(a).

The simplicity of Purcell's swimmer allows for a detailed examination of the impact of shear-thinning rheology on swimming. The above rationalization illustrates how changes in propulsion in a shear-thinning fluid may be qualitatively understood as a consequence of varying magnitudes of the shear-thinning effect along a swimmer and the resulting changes in the swimmer orientation.

C. Effect of unequal arm rotational rates

In a Newtonian fluid, due to the kinematic reversibility and linearity of the Stokes equation, the net displacement of Purcell's swimmer is independent of the arm rotational rates. Equal rotational rates are therefore typically prescribed for the two arms in Purcell's swimmer, which we followed in the results presented in Secs. III A and III B. However, for a shear-thinning fluid, we expect that one could exploit the nonlinearity of the rheological behavior by modulating the arm rotational rates to alter the net swimmer displacement. In particular, by prescribing unequal arm rotational rates, we anticipate that the symmetry breaking not only will lead to changes in the net horizontal swimmer displacement but also will induce net vertical swimmer displacement, which is exactly zero in a Newtonian fluid.

To test the above hypothesis, we simulate the dynamics of Purcell's swimmer with unequal arm rotational rates. The magnitudes of the rotational rates at the left and right arms relative to the

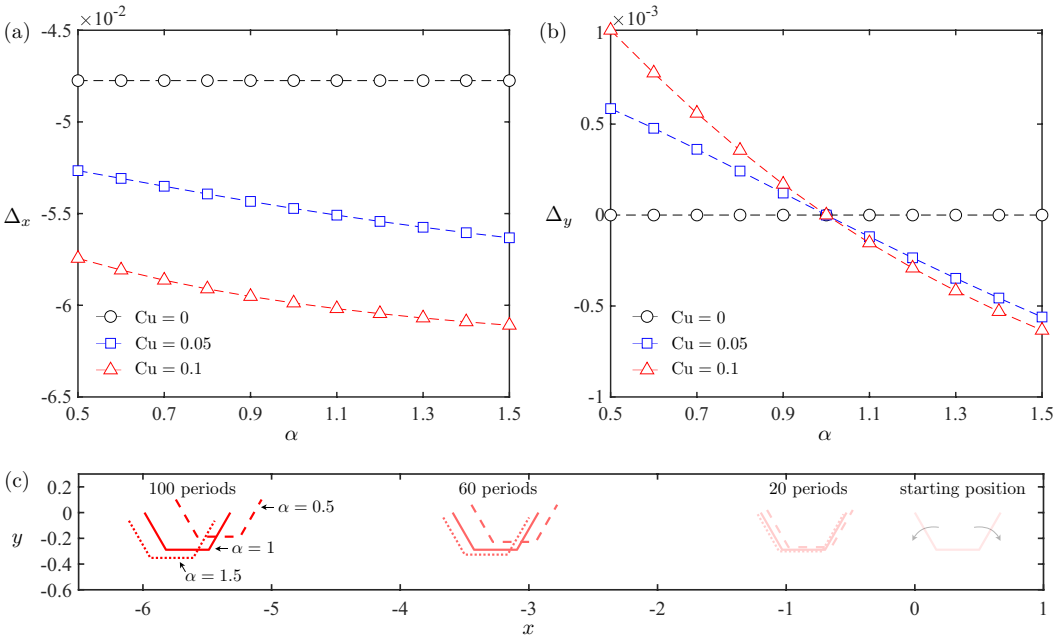

FIG. 4. The swimmer displacement in the (a) horizontal (Δ_x) and (b) vertical (Δ_y) directions as a function of the ratio of arm rotational rates α in Newtonian (Cu $= 0$) and shear-thinning (Cu $= 0.05$, Cu $= 0.1$) fluids. (c) Visualization of the displacement of swimmers with equal ($\alpha = 1$) and unequal ($\alpha = 0.5$ and $\alpha = 1.5$) arm rotational rates in a shear-thinning fluid (Cu $= 0.1$) after different numbers of periods. Here, $n = 0.25$.

middle link are denoted, respectively, as ω_1 and ω_2. Here, we use ω_2 in the definition of the Carreau number, $\mathrm{Cu} = \omega_2\lambda_C$, and a new dimensionless group measuring the ratio of the arm rotational rates, $\alpha = \omega_1/\omega_2$, emerges. We note that the stroke angle ϕ is kept constant, so that the time spent during the rotation of the left arm is different from that for the right arm. Figures 4(a) and 4(b) show the dynamics of Purcell's swimmer with unequal arm rotational rates ($\alpha \neq 1$) in a shear-thinning fluid. The results in Secs. III A and III B are recovered when $\alpha = 1$. In Fig. 4(a), the net horizontal swimmer displacement in a Newtonian fluid (Cu $= 0$, black circles) remains unaffected by the unequal arm rotational rates (varying α), as expected from the kinematic reversibility and linearity of the Stokes equation. The corresponding net vertical swimmer displacement remains zero for all values of α, as shown in Fig. 4(b). However, in a shear-thinning fluid (Cu $= 0.05$ and Cu $= 0.1$), the net horizontal swimmer displacement varies with the ratio of the arm rotational rates α. Moreover, we show in Fig. 4(b) that the symmetry breaking due to unequal arm rotational rates can, indeed, lead to net vertical swimmer displacement: When the left arm rotates faster than the right arm ($\alpha > 1$), Purcell's swimmer displaces in the negative y direction (downward), and the opposite holds for $\alpha < 1$. As a remark, while we anticipated that different magnitudes of the shear-thinning effect induced by unequal arm rotational rates would cause these net vertical displacements, a physical understanding of why they occur upward versus downward remains unclear to us. It is also observed from Fig. 4(b) that the magnitude of the resulting vertical displacement for $\alpha < 1$ and $\alpha > 1$ is not symmetric about $\alpha = 1$.

We visualize the displacement of Purcell's swimmer with various ratios of unequal arm rotational rates ($\alpha = 0.5$, $\alpha = 1$, and $\alpha = 1.5$) in a shear-thinning fluid (Cu $= 0.1$) after different numbers of periods in Fig. 4(c). The above results demonstrate that shear-thinning rheology can lead to both quantitative (modification of net horizontal displacement) and qualitative (new dynamics in the vertical direction) changes in the propulsion behaviors. In particular, the emergence of the new dynamics in the vertical direction, enabled by the nonlinear rheological behavior, adds versatility to

Purcell's swimmer by allowing more complex (two-dimensional) movements otherwise impossible in a Newtonian fluid.

IV. CONCLUDING REMARKS

In this work, we examined the impact of shear-thinning rheology on low-Reynolds-number locomotion via Purcell's swimmer. Through this canonical model swimmer, we demonstrated how shear-thinning rheology can modify both the magnitude and direction of propulsion depending on the details of the swimming strokes, including the stroke angle and the arm rotational rate. The simplicity of Purcell's swimmer allows us to rationalize how varying the magnitude of the shear-thinning effect along a swimmer leads to changes in the orientation of the linkage that favor the swimmer displacement in a particular direction. We also demonstrate how symmetry breaking due to unequal arm rotational rates can couple with the shear-thinning effect to induce net vertical swimmer displacements, which cannot occur in a Newtonian fluid. These findings suggest modulating the arm rotational rates as a way to exploit the non-Newtonian rheological behavior to enable different two-dimensional motions of Purcell's swimmer.

We remark on several limitations of the current study and suggest directions of future work. First, the use of a local drag model in this work addresses only the local influence due to changes in the viscosity in a shear-thinning fluid [37], without accounting for the nonlocal effect due to the change in the flow field around the swimmer [34,38,40,42]. The local approximations in both the flow and viscosity variations also limit the validity of the current model to the low-Carreau-number regime [37]. Considering future experimental realizations, for shear-thinning fluids made of xanthan gum solutions, typical λ_C can be on the order of 0.1–10 s with n in the range of 0.3–0.9, depending on the xanthan gum concentration in the solution [33,54]. With a typical rotation rate of 1 s^{-1} [46], the Carreau number can vary in the range $\mathrm{Cu} \sim O(0.1\text{–}10)$ or even higher in the experiments. Given these larger values of Cu, we expect the shear-thinning effect to be more significant in the experiments than that revealed by the low-Cu analysis here. However, subsequent investigations extending the study to larger Cu and accounting for both local and nonlocal shear-thinning effects are required to capture experimental measurements quantitatively. Finally, we considered in this work unequal but constant arm rotational rates. Further allowing the rotation rates to be functions of time could lead to more complex swimmer dynamics and new optimization problems for locomotion in complex fluids.

ACKNOWLEDGMENTS

Funding support from the National Science Foundation (Grants No. EFMA-1830958 and No. CBET-1931292) is gratefully acknowledged. We also acknowledge the computational resources from the WAVE computing facility enabled by the Wiegand Foundation at Santa Clara University.

[1] L. J. Fauci and R. Dillon, Biofluidmechanics of reproduction, Annu. Rev. Fluid Mech. **38**, 371 (2006).
[2] E. A. Gaffney, H. Gadêlha, D. J. Smith, J. R. Blake, and J. C. Kirkman-Brown, Mammalian sperm motility: Observation and theory, Annu. Rev. Fluid Mech. **43**, 501 (2011).
[3] S. A. Mirbagheri and H. C. Fu, *Helicobacter pylori* Couples Motility and Diffusion to Actively Create a Heterogeneous Complex Medium in Gastric Mucus, Phys. Rev. Lett. **116**, 198101 (2016).
[4] H. Gadêlha, P. Hernández-Herrera, F. Montoya, A. Darszon, and G. Corkidi, Human sperm uses asymmetric and anisotropic flagellar controls to regulate swimming symmetry and cell steering, Sci. Adv. **6**, eaba5168 (2020).
[5] B. J. Nelson, I. K. Kaliakatsos, and J. J. Abbott, Microrobots for minimally invasive medicine, Annu. Rev. Biomed. Eng. **12**, 55 (2010).
[6] J. L. Moran and J. D. Posner, Phoretic self-propulsion, Annu. Rev. Fluid Mech. **49**, 511 (2017).

[7] C. Hu, S. Pané, and B. J. Nelson, Soft micro- and nanorobotics, Annu. Rev. Control Rob. Auton. Syst. **1**, 53 (2018).
[8] Z. Wu, Y. Chen, D. Mukasa, O. S. Pak, and W. Gao, Medical micro/nanorobots in complex media, Chem. Soc. Rev. **49**, 8088 (2020).
[9] E. M. Purcell, Life at low Reynolds number, Am. J. Phys. **45**, 3 (1977).
[10] E. Lauga and T. R. Powers, The hydrodynamics of swimming microorganisms, Rep. Prog. Phys. **72**, 096601 (2009).
[11] J. M. Yeomans, D. O. Pushkin, and H. Shum, An introduction to the hydrodynamics of swimming microorganisms, Eur. Phys. J. Spec. Top. **223**, 1771 (2014).
[12] E. Lauga, *The Fluid Dynamics of Cell Motility*, Cambridge Texts in Applied Mathematics (Cambridge University Press, Cambridge, 2020).
[13] A. C. H. Tsang, E. Demir, Y. Ding, and O. S. Pak, Roads to smart artificial microswimmers, Adv. Intell. Syst. **2**, 1900137 (2020).
[14] B. Castaing, An introduction to hydrodynamics, in *Hydrodynamics and Nonlinear Instabilities*, edited by C. Godrèche and P. Manneville, Collection Alea-Saclay: Monographs and Texts in Statistical Physics (Cambridge University Press, Cambridge, 1998), pp. 25–80.
[15] L. E. Becker, S. A. Koehler, and H. A. Stone, On self-propulsion of micro-machines at low Reynolds number: Purcell's three-link swimmer, J. Fluid Mech. **490**, 15 (2003).
[16] J. E. Avron and O. Raz, A geometric theory of swimming: Purcell's swimmer and its symmetrized cousin, New J. Phys. **10**, 063016 (2008).
[17] Y. Or, Asymmetry and Stability of Shape Kinematics in Microswimmers' Motion, Phys. Rev. Lett. **108**, 258101 (2012).
[18] D. Tam and A. E. Hosoi, Optimal Stroke Patterns for Purcell's Three-Link Swimmer, Phys. Rev. Lett. **98**, 068105 (2007).
[19] O. Wiezel and Y. Or, Optimization and small-amplitude analysis of Purcell's three-link microswimmer model, Proc. R. Soc. A **472**, 20160425 (2016).
[20] L. Giraldi, P. Martinon, and M. Zoppello, Optimal design of Purcell's three-link swimmer, Phys. Rev. E **91**, 023012 (2015).
[21] E. Passov and Y. Or, Dynamics of Purcell's three-link microswimmer with a passive elastic tail, Eur. Phys. J. E **35**, 78 (2012).
[22] K. Ishimoto, C. Moreau, and K. Yasuda, Self-organized swimming with odd elasticity, Phys. Rev. E **105**, 064603 (2022).
[23] R. L. Hatton, Y. Ding, H. Choset, and D. I. Goldman, Geometric Visualization of Self-Propulsion in a Complex Medium, Phys. Rev. Lett. **110**, 078101 (2013).
[24] H. C. Berg, How spiroplasma might swim. J. Bacteriol. **184**, 2063 (2002).
[25] G. J. Elfring and E. Lauga, Theory of locomotion through complex fluids, in *Complex Fluids in Biological Systems*, edited by S. E. Spagnolie (Springer, New York, 2015), pp. 283–317.
[26] J. Sznitman and P. E. Arratia, Locomotion through complex fluids: An experimental view, in *Complex Fluids in Biological Systems*, edited by S. E. Spagnolie (Springer, New York, 2015), pp. 245–281.
[27] D. A. Fedosov, H. Noguchi, and G. Gompper, Multiscale modeling of blood flow: From single cells to blood rheology, Biomech. Model. Mechanobiol. **13**, 239 (2014).
[28] S. H. Hwang, M. Litt, and W. C. Forsman, Rheological properties of mucus, Rheol. Acta **8**, 438 (1969).
[29] T. D. Montenegro-Johnson, A. A. Smith, D. J. Smith, D. Loghin, and J. R. Blake, Modelling the fluid mechanics of cilia and flagella in reproduction and development, Eur. Phys. J. E **35**, 111 (2012).
[30] T. D. Montenegro-Johnson, D. J. Smith, and D. Loghin, Physics of rheologically enhanced propulsion: Different strokes in generalized stokes, Phys. Fluids **25**, 081903 (2013).
[31] M. Dasgupta, B. Liu, H. C. Fu, M. Berhanu, K. S. Breuer, T. R. Powers, and A. Kudrolli, Speed of a swimming sheet in Newtonian and viscoelastic fluids, Phys. Rev. E **87**, 013015 (2013).
[32] J. R. Vélez-Cordero and E. Lauga, Waving transport and propulsion in a generalized Newtonian fluid, J. Non-Newton. Fluid Mech. **199**, 37 (2013).
[33] D. A. Gagnon, N. C. Keim, and P. E. Arratia, Undulatory swimming in shear-thinning fluids: Experiments with Caenorhabditis elegans, J. Fluid Mech. **758**, R3 (2014).

[34] G. Li and A. M. Ardekani, Undulatory swimming in non-Newtonian fluids, J. Fluid Mech. **784**, R4 (2015).
[35] D. A. Gagnon and P. E. Arratia, The cost of swimming in generalized Newtonian fluids: Experiments with C. elegans, J. Fluid Mech. **800**, 753 (2016).
[36] J.-S. Park, D. Kim, J. H. Shin, and D. A. Weitz, Efficient nematode swimming in a shear thinning colloidal suspension, Soft Matter **12**, 1892 (2016).
[37] E. E. Riley and E. Lauga, Empirical resistive-force theory for slender biological filaments in shear-thinning fluids, Phys. Rev. E **95**, 062416 (2017).
[38] S. Gómez, F. A. Godínez, E. Lauga, and R. Zenit, Helical propulsion in shear-thinning fluids, J. Fluid Mech. **812**, R3 (2017).
[39] Z. Qu and K. S. Breuer, Effects of shear-thinning viscosity and viscoelastic stresses on flagellated bacteria motility, Phys. Rev. Fluids **5**, 073103 (2020).
[40] E. Demir, N. Lordi, Y. Ding, and O. S. Pak, Nonlocal shear-thinning effects substantially enhance helical propulsion, Phys. Rev. Fluids **5**, 111301(R) (2020).
[41] C. Datt, L. Zhu, G. J. Elfring, and O. S. Pak, Squirming through shear-thinning fluids, J. Fluid Mech. **784**, R1 (2015).
[42] K. Pietrzyk, H. Nganguia, C. Datt, L. Zhu, G. J. Elfring, and O. S. Pak, Flow around a squirmer in a shear-thinning fluid, J. Non-Newton. Fluid. **268**, 101 (2019).
[43] Y. Chen, E. Demir, W. Gao, Y.-N. Young, and O. S. Pak, Wall-induced translation of a rotating particle in a shear-thinning fluid, J. Fluid Mech. **927**, R2 (2021).
[44] B. van Gogh, E. Demir, D. Palaniappan, and O. S. Pak, The effect of particle geometry on squirming through a shear-thinning fluid, J. Fluid Mech. **938**, A3 (2022).
[45] K. Qin, Z. Peng, Y. Chen, H. Nganguia, L. Zhu, and O. S. Pak, Propulsion of an elastic filament in a shear-thinning fluid, Soft Matter **17**, 3829 (2021).
[46] T. Qiu, T.-C. Lee, A. G. Mark, K. I. Morozov, R. Münster, O. Mierka, S. Turek, A. M. Leshansky, and P. Fischer, Swimming by reciprocal motion at low Reynolds number, Nat. Commun. **5**, 5119 (2014).
[47] K. Han, C. W. Shields, B. Bharti, P. E. Arratia, and O. D. Velev, Active reversible swimming of magnetically assembled "microscallops" in non-Newtonian fluids, Langmuir **36**, 7148 (2020).
[48] J. Gray and G. J. Hancock, The propulsion of sea-urchin spermatozoa, J. Exp. Biol. **32**, 802 (1955).
[49] J. Lighthill, *Mathematical Biofluiddynamics* (SIAM, Philadelphia, 1975).
[50] R. B. Bird, R. C. Armstrong, and O. Hassager, *Dynamics of Polymeric Liquids*, Fluid Mechanics (Wiley, New York, 1987), Vol. 1.
[51] Y. Cho and K. Kensey, Effects of the non-Newtonian viscosity of blood on flows in a diseased arterial vessel. Part 1: Steady flows, Biorheology **28**, 241 (1991).
[52] F. J. H. Gijsen, F. N. van de Vosse, and J. D. Janssen, The influence of the non-Newtonian properties of blood on the flow in large arteries: Steady flow in a carotid bifurcation model, J. Biomech. **32**, 601 (1999).
[53] W. G. Li, X. Y. Luo, S. B. Chin, N. A. Hill, A. G. Johnson, and N. C. Bird, Non-Newtonian bile flow in elastic cystic duct: One- and three-dimensional modeling, Ann. Biomed. Eng. **36**, 1893 (2008).
[54] U. Eberhard, H. J. Seybold, M. Floriancic, P. Bertsch, J. Jiménez-Martínez, J. S. Andrade, and M. Holzner, Determination of the effective viscosity of non-Newtonian fluids flowing through porous media, Front. Phys. **7**, 71 (2019).
[55] M. J. D. Powell, A hybrid method for nonlinear equations, in *Numerical Methods for Nonlinear Algebraic Equations*, edited by P. Rabinowitz (Gordon and Breach, London, 1970).
[56] L. Petzold, Automatic selection of methods for solving stiff and nonstiff systems of ordinary differential equations, SIAM J. Sci. Comput. **4**, 136 (1983).
[57] A. C. Hindmarsh, ODEPACK, a systematized collection of ODE solvers, in *Scientific Computing*, edited by R. S. Stepleman *et al.* (North-Holland, Amsterdam, 1983).